CHAPTER 4

Interfacial phenomena during Fenton reaction on starch stabilized magnetite nanoparticles: molecular dynamics and experimental investigations

4.1 Introduction

Fenton reactions are eco-friendly advanced oxidation processes for the degradation of harmful organic contaminants from wastewater [Kurian & Nair (2015), Wang et al. (2016)]. Typically, homogeneous Fenton reaction involves catalytic production of the hydroxyl radicals by reduction of hydrogen peroxide. The hydroxyl radicals are highly efficient but non-selective oxidants. There are two main parts of the mechanism, and the first step is the relatively faster H_2O_2 reduction by Fe^{2+} ions. The next reverse reaction of Fe^{3+} reduction to Fe^{2+} is the rate-limiting one, with the overall process requiring an acidic pH~3. The need to neutralize the pH of the effluent before release and substantial sludge formation makes the process quite inefficient at larger scales. In contrast to this, heterogeneous catalysts for Fenton processes are more stable and maintained over many cycles.

As discussed earlier in chapter 1, a large amount of research concentrates on finding better catalyst materials for this industrially critical reaction, but still few unresolved questions regarding its mechanism. Wang et al. (2016), Liang et al. (2012), Yang et al. (2009) proposed a Langmuir-Hinshelwood like mechanism; other researchers Liang et al. (2012) and Furman et al. (2009) suggested that an Eley-Rideal type pathway may be operational. One opinion is that the produced hydroxyl radicals attack the substrate molecules adsorbed on the catalyst surface. But the excess adsorption of the organic substrate on the catalyst surface also decreases the hydroxyl radical production in the Fenton catalysis [Xue et al. (2009)]. Keeping in view the short lifetime of the hydroxyl radicals, a variation of this proposal was that the oxidants mainly attack organic species near the catalyst surface [He et al. (2014)]. The research groups Lücking et al. (1998) and Oliveira et al. (2007) hinted that the competition between the target organic compounds and H_2O_2 molecules for active sites might impede the Fenton reaction proposed and an

Eley-Rideal type mechanism. [He et al. (2016)] nicely summarizes in review based on the perspectives of the interfacial mechanisms on the Fenton reaction catalyst surface but makes it clear that the problem remains unresolved.

The resolution of these aspects of the surface adsorption mechanism can enable the design of a better version of a particular catalyst, significantly enhancing its Fenton reactivity. The experimental investigation of the facets of the interfacial mechanism is complicated because of the large number of coupled variables involved. Hence, this chapter combines classical MD investigations with proper experimental research to elucidate the Fenton interfacial mechanism on the surface of magnetite nanoparticles.

Several iron minerals and iron oxide/hydroxides have demonstrated heterogeneous Fenton catalytic activity [Yan et al. (2012), Wang & Huang (2011), Guo et al. (2010) and Nie et al. (2008)]. Out of these, the magnetic properties of the spinel structured magnetite (Fe_3O_4) phase makes it a more attractive Fenton catalyst for the degradation of various organic pollutants [He et al. (2015), Xue et al. (2009), Wang et al. (2013), Sun & Lemley (2011), (Xu & Wang (2012)]. MNPs below a critical size become superparamagnetic, making them easy to separate magnetically. Such nanoparticles can be re-dispersed in a new reaction system after removing the external magnetic field and efficiently re-used several times. Nevertheless, some investigations on magnetite nanoparticles as the Fenton catalysts have reported that organic substrates can cause aggregation by surface oxidation on repeated use [Wei & Wang (2008)].

Suitable stabilization of MNPs can solve these problems. Thus different workers have used organic moiety, surfactants, polymers, biomolecules, inorganic compounds, and carbon materials to alter the [Niu et al. (2011), Leng et al. (2013), Shin et al. (2008), Sun et al. (2016), Li et al. (2018b)] surface properties of MNPs. Interestingly, attaching a suitable chelating agent or a polymeric stabilizer to the magnetite surface can also make

the Fenton catalyst considerably more effective [Zhou et al. (2018), Wang et al. (2016)]. Soluble starch (amylose) is an economical, hydrophilic, and natural biodegradable polymer [Avella et al. (2005)]. It is already known as an efficient stabilizing agent for MNPs [Jiang et al. (2009), Abdullah et al. (2017), Zhang et al. (2011), Tancredi et al. (2015)]. But the Fenton activity of starch stabilized magnetite nanoparticles (SMNPs) has still not been investigated for PNP degradation. The two main functional groups in soluble starch (amylose) are the hydroxyl group and the acetal group, which can bond with magnetite to provide it with better physical and colloidal stability [He & Zhao (2005), Zhang et al.(2010), An et al. (2011)]. These groups may also be useful in making nano-magnetite a more efficient Fenton catalyst.

Given the above discussion, the present chapter investigates the Fenton degradation of PNP on MNPs and SMNPs catalysts experimentally and through MD simulations. Hence, the interfacial distribution of chemical species from MD simulations, combined with experimental results, were used to understand the heterogeneous Fenton mechanism. Such a holistic approach for understanding the interfacial phenomena on a Fenton nanocatalyst surface has not been reported previously.

Parallelly, MD simulations were carried out under constant pressure conditions to understand the interfacial Fenton mechanism on magnetite and starch stabilized magnetite nanoparticles. These MD investigations focused on the competitive adsorption of H_2O_2 and PNP on the MNP surface in the presence of a large number of solvent water molecules. Another model studied the adsorption of H_2O_2 and PNP on an SMNP under the same conditions through MD simulations. The presence of starch changed the distribution of various molecules around the SMNP completely, which enabled us to infer the reason for substantially better Fenton kinetics on SMNPs.

4.2 Methodology

4.2.1 Simulation Models

A suitable supercell was constructed from the inverse spinel face-centered cubic (FCC) unit cell of magnetite (Fe_3O_4) (from the Crystallography Open Database entry number: 907644 [Fleet (1981)]. A cluster of 149 atoms was carved out of it by using the MAPS software. The diameter of this magnetite nanocluster was 1.4 nm. The magnetite nanocluster was placed in the center of a 60Å×60Å×60Å cubic simulation box (Figure 4.1a).

For the starch stabilized magnetite model, an amylose unit composed of $C_{30}H_{52}O_{26}$ molecular formula was constructed using the molecular builder in the MAPS software. The amylose unit was optimized by Modified Neglect of Diatomic Overlap with d-orbitals (MNDO/d) [Thiel & Voityuk (1992)] semi-empirical approach. Then six amylose units were placed close to the magnetite cluster and after an initial optimization run, another MD equilibration run of ~1 nanosecond was used to adsorb the amylose on to the magnetite cluster surface (Figure 4.1b).

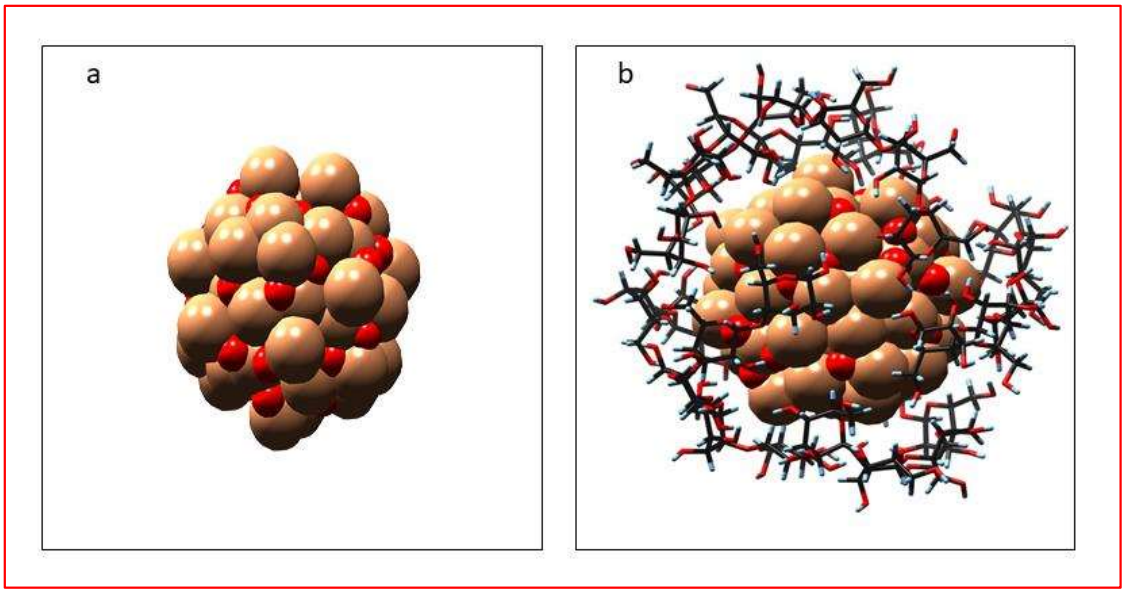

Figure 4.1 a) Magnetite nanocluster model and b) Starch stabilized magnetite nanocluster model used in MD simulations.

Water, PNP, and H_2O_2 molecules were constructed using the molecule builder in MAPS, and their molecular geometries were optimized by MNDO/d. Water molecules modified by TIP4P charges and angles from Jorgensen et al. (1983) were used. The Amorphous builder plugin in MAPS was employed to insert 30 PNP, 100 H_2O_2, and 2000 water molecules into magnetite cluster and starch stabilized magnetite cluster models such that the initial densities of the systems were ~1g/cc. The magnetite cluster and the starch stabilized magnetite cluster models after the insertion of PNP, H_2O_2 and water molecules are abbreviated by MC and SMC in the rest of this chapter.

4.2.2 Simulation Method

MD simulations were performed on MC and SMC models using the SciPCFF force field, a modified version of the PCFF force field [Sun et al. (1994)]. The SciPCFF force field (developed by Scienomics Inc) incorporates 9-6 Van der Waals forces and bond increment parameters of various compounds from the COMPASS force field already published in the literature. Table 4.1 in supporting information gives the L-J parameters used in this research.

LAMMPS) package [Plimpton (1995)] was used for carrying out these NPT ensemble MD simulations. The two systems were simulated under periodic boundary conditions. The simulations were carried out for 10 nanoseconds with time step 1 femtosecond at a constant 1bar pressure and 298K temperature. Nose-Hoover thermostat [Nosé, (1984), Hoover, (1985)] was used for pressure and temperature control with 10 femtoseconds damping. The cut-off for nonbonded interactions was 12 Å, and the particle mesh approach was used to calculate Coulomb interactions. Both systems were subjected to 7 nanoseconds equilibration and a subsequent production run time of 3 nanoseconds.

Table 4.1 LJ 9-6 Potential Parameters used in MD simulations.

Atom type	ϵ_0 (kcal/mol)	r_0 (Å)
cp (carbon attached to the benzene ring in PNP)	0.119	3.426
n3o (Nitrogen atom of the nitro group present in PNP)	0.081	3.28
o12 (Oxygen atom of the nitro group present in PNP)	0.081	2.97
o* (Oxygen atom in water)	0.132	3.168
Fe (Iron atom in magnetite)	0.83	3.56
Ox (Oxygen atom in magnetite)	0.132	3.168
hc (hydrogen attached to the carbon atom in PNP)	0.038	2.51
Oh (Oxygen atom of OH group in PNP)	0.162	3.172
Ho (Hydrogen atom of OH group in PNP)	0.0135	0.949
Oc (Oxygen atom making the glycosidic linkage in the amylose)	0.162	2.882
c3 (carbon atom attached to the primary –OH group in amylose)	0.114	3.332

The interaction energies of MC and SMC systems [Zhang et al. (2019), Lan et al. (2019), Gao et al. (2020)] were also computed for better understanding. The interaction energy (E_{IE}) is defined as the difference between the (long time average) potential energy of the final system (E_{final} of MC or SMC) and the sum of (long time average) potential energies of the component systems ($E_{magnetite/Starch\ stabilized\ magnetite\ cluster} + E_{Solvent(H2O2+water+PNP)}$).

Therefore, the below formula defines the interaction energies for MC and SMC systems.

$$E_{IE} = E_{(MC/SMC\ system)} - (E_{magnetite/Starch\ stabilized\ magnetite\ cluster} + E_{Solvent(H2O2+water+PNP)}) \quad (4.1)$$

4.2.3 Experimental methodology

Superparamagnetic MNPs and SMNPs were prepared as per the protocol reported by Singh et al. (2016). Materials used in the synthesis were analytical grade iron (II) sulfate heptahydrate (Merck), NaOH (Merck), and starch. First, a 0.2M aqueous solution of iron (II) sulfate heptahydrate was prepared. For SMNPs preparation, a mixture of appropriate amounts of starch and 0.2M aqueous solution of iron (II) sulfate heptahydrate were mixed. The respective solutions (depending on whether it was MNPs or SMNPs synthesis) were then added in a drop-wise manner into separate 0.4M NaOH solutions at 80^{o}C with constant stirring. After completing the addition, the two reaction mixtures were heated at 80^{o}C for two more hours until dark black precipitates were formed. These precipitates were separated by magnetic decantation, repeatedly washed until neutral, and then dried at 40^{o}C in a hot air oven.

4.2.4 Catalytic degradation of *p*-nitrophenol

About 7.5 mg of the respective catalyst was added to 10mL of the PNP solution (179μM) at pH 3. The suspension was then allowed to stand for 60 minutes for possible adsorption of PNP on the nanoparticles in the sample considered. Next, 10mL of 25mM H_2O_2 (Merck) solution was added to this suspension. The reaction took place in the dark at room temperature (25^{0}C). The UV-visible spectrum of the PNP solution (after removing the nanoparticles) was measured at regular intervals. The maximum absorbance of the spectrum was at 317 nm wavelength. Hereafter, A_0 denotes this absorbance of the

PNP solution (at 317 nm) at the initial time, and A represents the same recorded at subsequent time intervals.

4.3 Results and Discussion

4.3.1 Experimental results

Figure 4.2 shows the XRD plots of the MNPs and SMNPs samples. All peaks in the MNPs XRD also occur in the SMNPs pattern There were no other peaks. In both cases, there was the formation of only a pure magnetite phase.

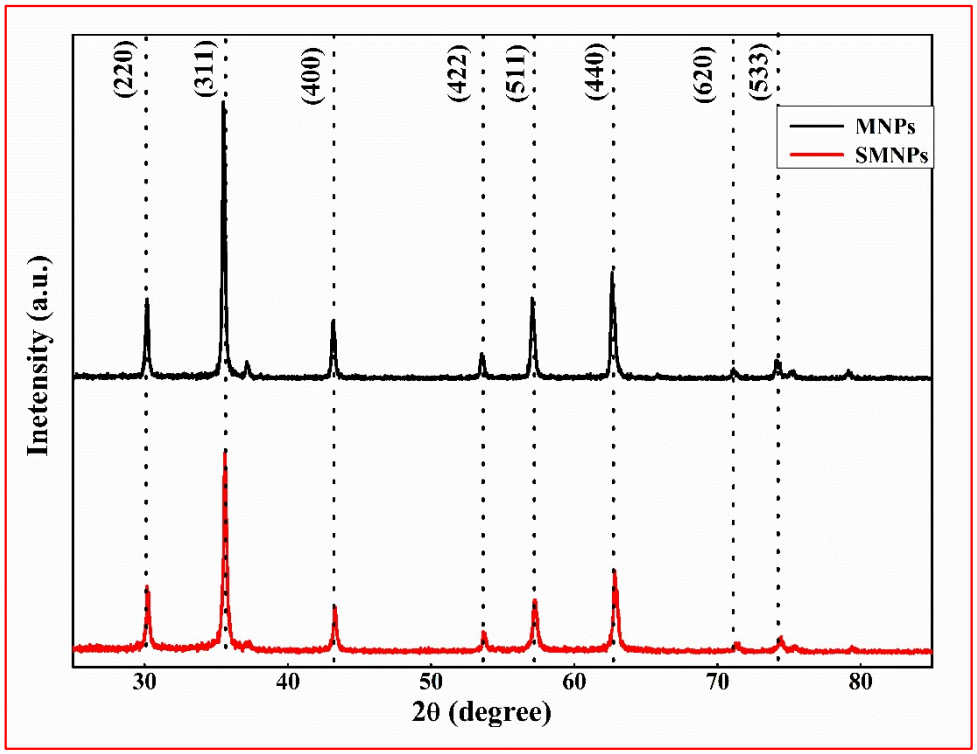

Figure 4.2 The XRD patterns of powder samples MNPs and SMNPs.

Figures 4.3a and 4.3b display the SEM micrographs of MNPs and SMNPs samples, respectively. The SMNPs average particle sizes were smaller (than those in the MNPs sample) due to starch stabilization.

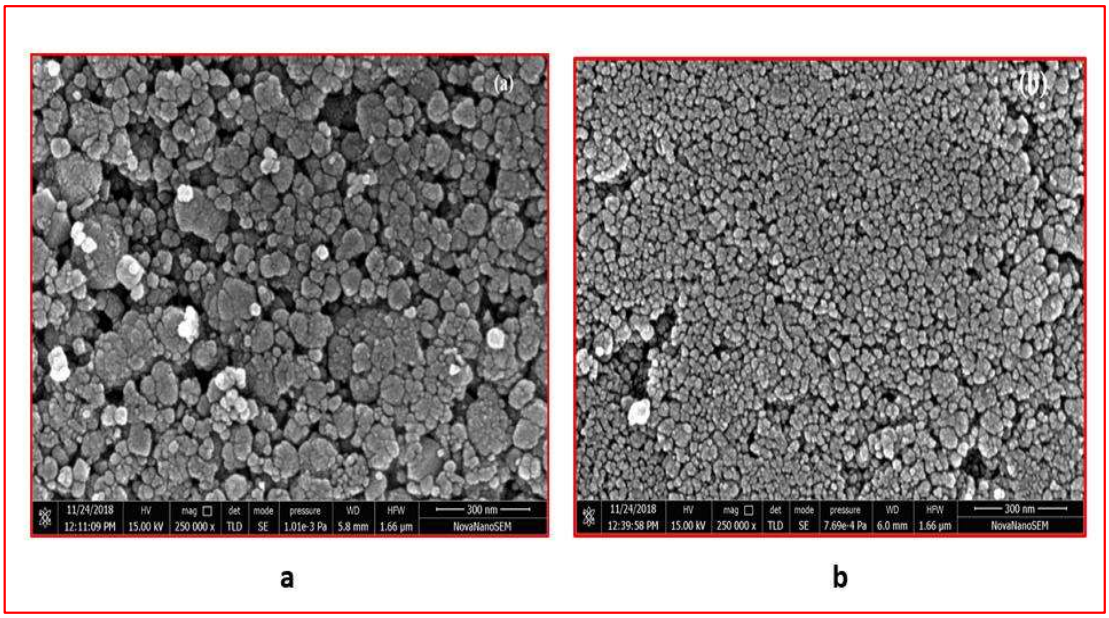

Figure 4.3 Representative SEM images of a) MNPs and b) SMNPs.

Figure 4.4 shows the UV-visible spectrum of a mixture of H_2O_2 and PNP in the presence of starch. There was no change in the UV-visible spectrum with time, confirming that soluble starch alone does not have any Fenton catalytic activity.

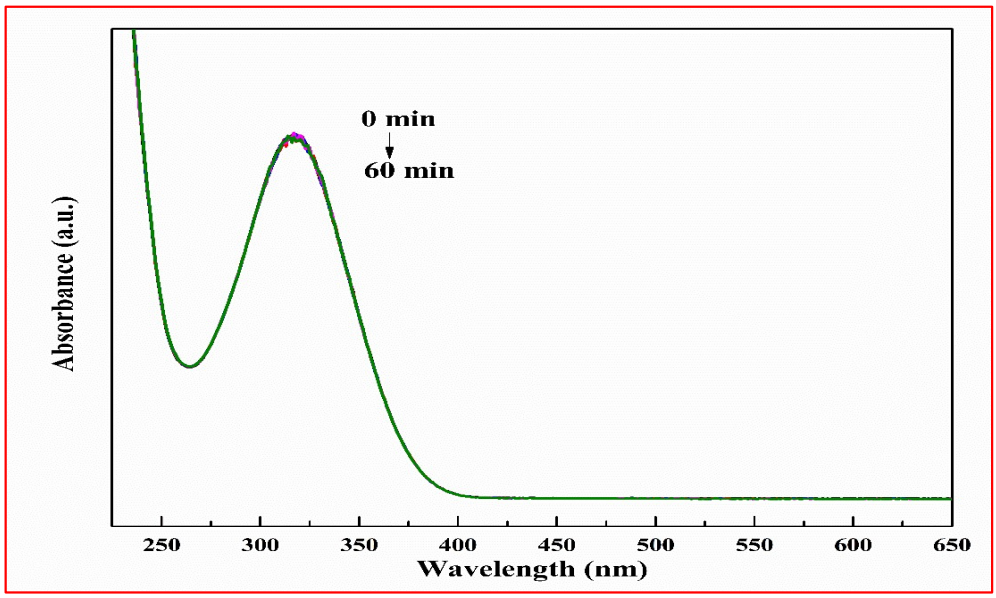

Figure 4.4 UV-visible plots of degradation of PNP at regular intervals of reaction time in the presence of only starch and H_2O_2 (without catalyst).

Figures 4.5a and 4.5b give the change in the UV-visible spectra of PNP with increasing time when the reaction was done in the presence of catalyst samples MNPs and SMNPs, respectively. Even after 210 minutes of reaction time, the degradation of only a small percentage of PNP took place when MNPs was the catalyst. The reaction catalyzed by SMNPs demonstrated a much better result. In this case, almost all of the PNP got degraded in only 80 minutes of reaction time. Both degradations follow first-order kinetics (Figure 4.5c), indicating that the mechanism remained the same in both cases.

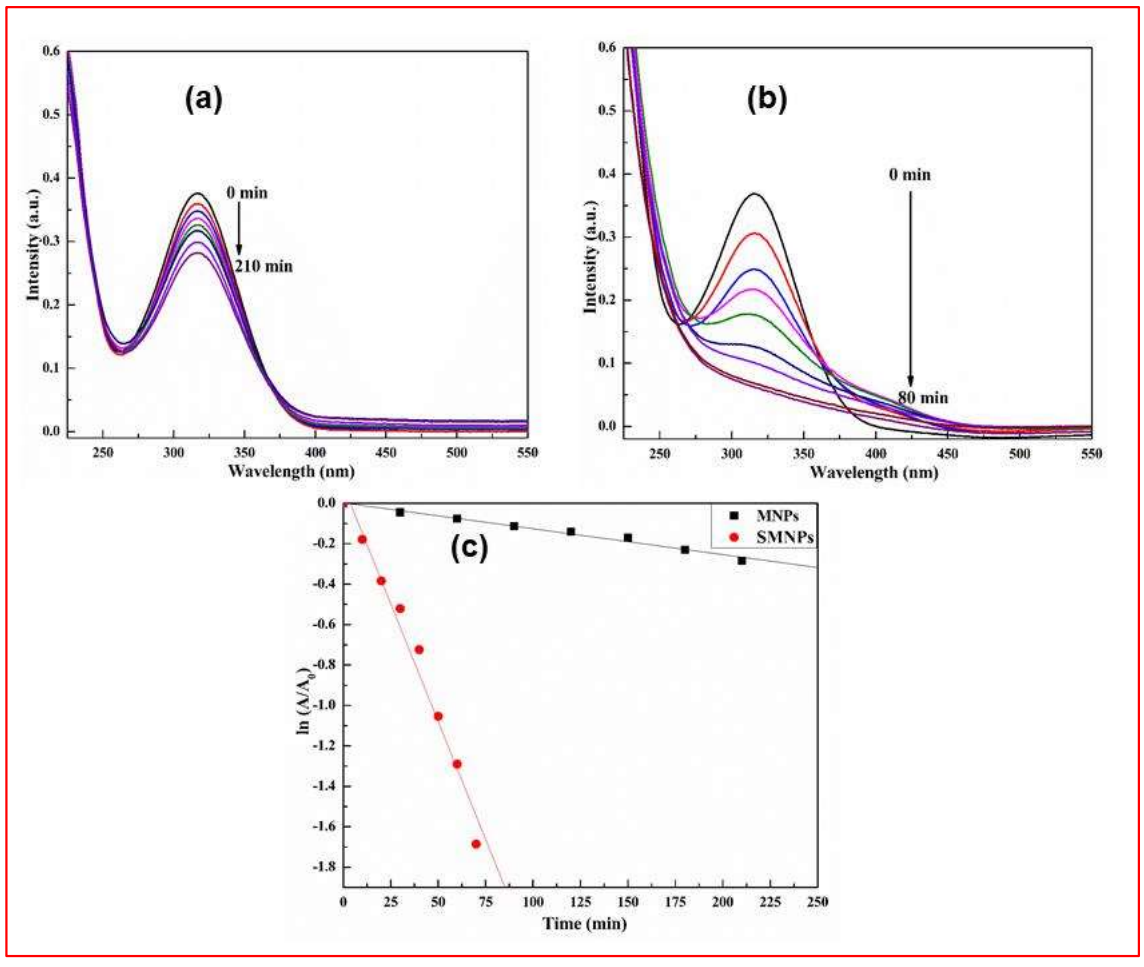

Figure 4.5 UV-visible absorbance plots of Fenton degradation of PNP at regular intervals of reaction time (under dark conditions) catalyzed by a) MNPs and b) SMNPs samples, respectively. c) The plots of $\ln(A/A_0)$ [absorbance (A) measured at λ_{max} 317 nm] versus time for (PNP degradation) reactions catalyzed by SMNPs and MNPs nanocatalyst.

Starch stabilization of the magnetite nanoparticles reduces their sizes [Zhang et al. (2011)]. As mentioned earlier, soluble starch does not catalytically activate H_2O_2 molecules (Figure 4.4). Only the magnetite surface is an active catalyst for the Fenton reduction of H_2O_2 molecules. Therefore, starch molecules attached to the magnetite surface block many catalysts sites responsible for H_2O_2 activation. While a decrease in nanoparticle size increases the surface area, starch functionalization also decreases the number of catalyst sites available on the magnetite surface. Hence, overall, the two effects neutralize each other, and there is no net gain (in magnetite surface catalyst sites) due to starch stabilization induced nanoparticle size reduction.

4.3.2 MD results

This section attempts to understand the effect of starch stabilization on the PNP and H_2O_2 spatial distribution in the proximity of SMNPs by classical MD simulations. The first step for this is to find the spatial distribution of PNP and H_2O_2 around a magnetite nanoparticle and then compare it with the distribution after starch stabilization. Figure 4.6a gives a snapshot of the last MC system configuration obtained at the end of the production run. The blue circles indicate PNP molecules in this figure. Qualitatively, it appears that mainly PNP molecules surround the magnetite cluster. Figure 4.6b displays center of mass-RDF(CM-RDF) plots between H_2O_2 and magnetite cluster, and also between PNP and the magnetite cluster CM. These plots give a quantitative description of the spatial distribution of H_2O_2 and PNP around the magnetite cluster. The first peak of the PNP CM-RDF is closer to the magnetite cluster than that of the CM-RDF H_2O_2 curve. Also, the height of the first peak of the PNP RDF is much higher than the corresponding H_2O_2 peak. Thus, these plots give us the information that a layer of PNP molecules first surrounds the magnetite cluster, while the H_2O_2 units are distributed in the rest of the system.

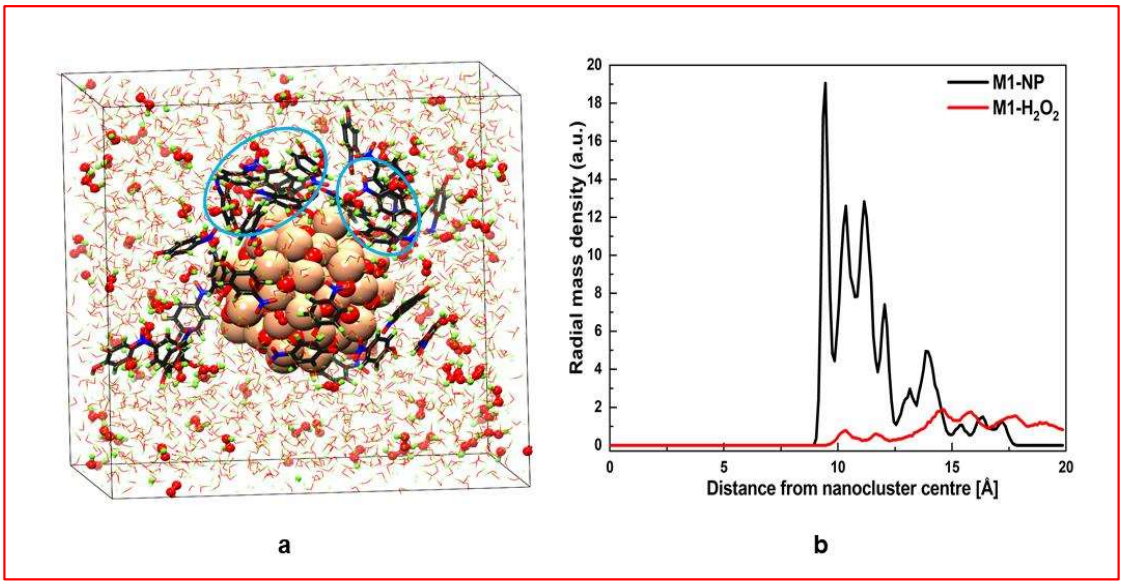

Figure 4.6. a) Snapshot shows adsorption of PNP on the magnetite cluster b) The CM-RDF profiles of H_2O_2 and PNP molecules calculated from the center of mass of the magnetite cluster. (Note that the magnetite cluster is abbreviated by M1 in b).

Figure 4.7a depicts the snapshot of PNP, and H_2O_2 molecules with the starch stabilized magnetite cluster in the SMC system. The green circles in figure 4.7a represent the location of H_2O_2 molecules near the starch stabilized magnetite cluster. The results are almost the opposite of that observed in the MC system. Now mainly H_2O_2 units make the first layer around the starch stabilized magnetite cluster. The CM-RDF profile of H_2O_2 from the center of the starch stabilized magnetite cluster (Figure 4.7b) shows an intense peak just adjacent to its surface. The CM-RDF first peak for the PNP molecules lies slightly to the right of the initial H_2O_2 peak.

Additionally, the intensity of the first peak of H_2O_2 is much higher than the corresponding PNP peak. Hence, a layer of H_2O_2 molecules surrounds the SMC unit with some PNP molecules as well in the vicinity.

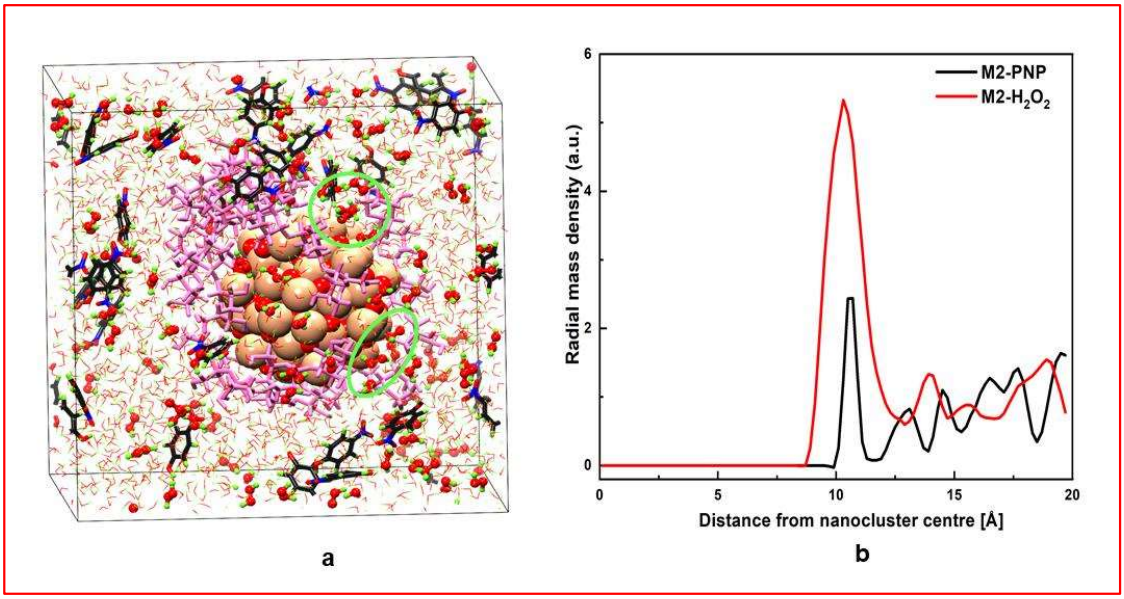

Figure 4.7 (a) Snapshot showing the distribution of H_2O_2 and PNP around the starch stabilized magnetite unit and b) The CM-RDF profiles of H_2O_2 and PNP from the center of starch stabilized magnetite cluster. (Note that the starch stabilized magnetite cluster is abbreviated by M2 in b).

Figure 4.8 shows the RDF plots (of systems MC and SMC, respectively) among various atom types from MC (surface) and those in the other three chemical species (PNP, H_2O_2, and H_2O). These plots investigate the nature of intermolecular interactions between (Fe and O) atoms in Fe_3O_4 and those making PNP, H_2O_2, or H_2O. Table 4.2 summarizes the atom type naming convention followed in these two figures. The first interaction peaks in these plots represent the most substantial nonbonded interaction dominating the proceedings. The first peak in Figure 4.8a is that between the O of Fe_3O_4 and H of the hydroxyl functional group in PNP (at ~1.5 Å). Thus, PNP interacts with the magnetite cluster mainly through this hydrogen bond. Another, much smaller peak, occurs at almost the same distance and is between the O of Fe_3O_4 and H of H_2O, indicating the first solvation shell of water around the magnetite unit. All other interactions have peaks at more considerable distances. There was little interaction between the oxygen of magnetite and hydrogen of H_2O_2 (shown by dashed purple lines in Figure 4.8a) at less than 5 Å

distance. A minimal (pink) peak depicting the average distance between Fe and oxygen of H_2O_2 only starts emerging near 3.2 Å. Therefore, PNP molecules make the immediate surroundings of the MC unit.

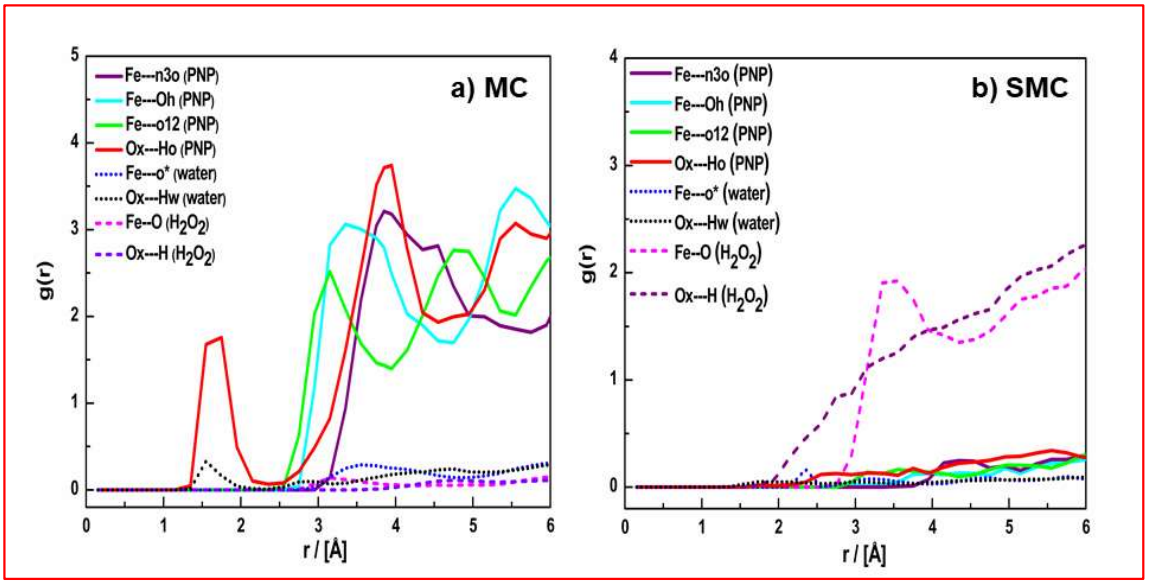

Figure 4.8. RDF plots displaying the interaction of different atoms present in the PNP, water, and H_2O_2 with those in a) MC and b) SMC system respectively.

Figure 4.8b plots the RDF between atom types in starch stabilized Fe_3O_4 and those in other PNP, H_2O_2 and H_2O species in system SMC. In the SMC model, there is a strong peak around 3.5 Å due to the interaction between Fe and O of H_2O_2. The first intense RDF peak emerges at a distance farther (than that observed in Figure 4.8a) because here, starch is in the space between the MC and the rest of the molecules in the solution phase. Hence, H_2O_2 molecules are interacting with the amylose units (of starch).

Table 4.2 The naming convention followed in the RDF plots given in figures 4.8 and 4.10.

Atom type names	Meaning
Fe	The iron atom in magnetite
Ox	The oxygen atom in magnetite
o*	The oxygen atom in the H_2O molecule
Hw	The hydrogen atom of H_2O molecule
O	An oxygen atom in H_2O_2
H	A hydrogen atom in H_2O_2
Oh	The oxygen atom of the OH group in PNP
Ho	The hydrogen atom of the OH group in PNP
o12	The oxygen atom of the nitro group present in PNP
n3o	The nitrogen atom of the nitro group present in PNP
Oc	The oxygen atom making the glycosidic linkage in the amylose unit
oR	The oxygen atom in the primary –OH group present in amylose
o2	The oxygen atom in a secondary –OH group of amylose
c3	The carbon atom attached to the primary –OH group in amylose

Figure 4.9 shows different atom types in an amylose unit. The last four rows in Table 4.1 lists the symbols denoting these atom types. Note that there are primary and secondary -OH groups at different carbon positions in an amylose unit.

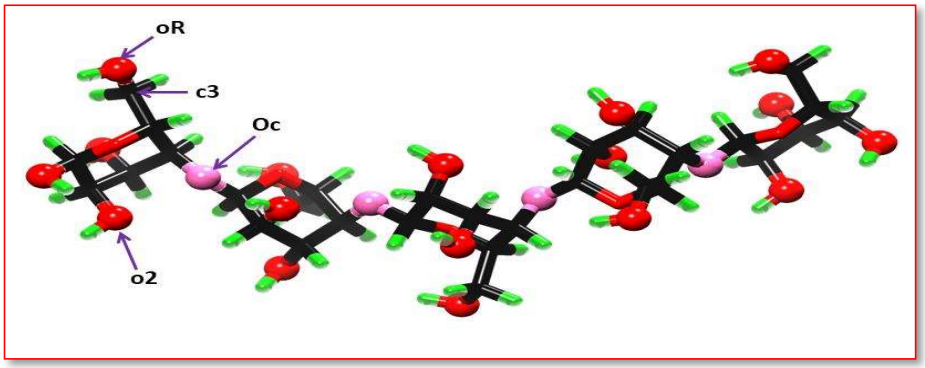

Figure 4.9 Atom type representation in an amylose unit.

Figure 4.10 presents the RDFs between various atom types of starch (functionalizing magnetite), H_2O_2, PNP, and water molecules for understanding the interactions involved. The RDF plot (Figure 4.10a) between atom type oR (the oxygen of the primary –OH group) and H (hydrogen of H_2O_2) shows a maximum near 3.0 - 3.5 Å (the green plot). The peak of the RDF between the (primary –OH group) carbon (atom type c3) and the oxygen of H_2O_2 occurs at a slightly longer 4 Å distance (solid pink line plot (in Figure 4.10b)). Note the maximum of this plot is the highest (among all graphs in this figure), but it is at 4 Å distance. Since the atom type oR and c3 are nearest neighbors (covalently bound), therefore the RDF between c3 and the oxygen of H_2O_2 is primarily a consequence of the oR-H interaction (the green RDF plot). Another aspect is that the green RDF plot (Figure 4.10a) is quite broad and begins from a distance that is near 2 Å in contrast to the pink plot (Figure 4.10b starting from 3 Å). Thus, the area under the

green RDF peak is more. Therefore, the H_2O_2 molecules predominate the neighborhood of the SMC through the oR-H interaction.

A peak of the RDF (Fig. 4.10c black dashed line) between the oR atom type and the nitrogen (atom type n3o) of PNP molecules also occurs at the 4 Å distance (shown in Figure 4.10c). Thus, PNP molecules are also in the proximity of the SMC cluster but not as close as the H_2O_2 units. The RDF peak (in Figure 4.10d) between the hydrogen of H_2O_2 and the oxygen of secondary OH groups (atom type o2) is also at 4 Å, but its peak height is much lesser. Finally, water molecules wet the amylose unit through interaction between the oxygen of the primary hydroxyl group and the hydrogen of H_2O. But these RDF plots are of considerably lesser intensity than the other graphs in Figure 4.10.

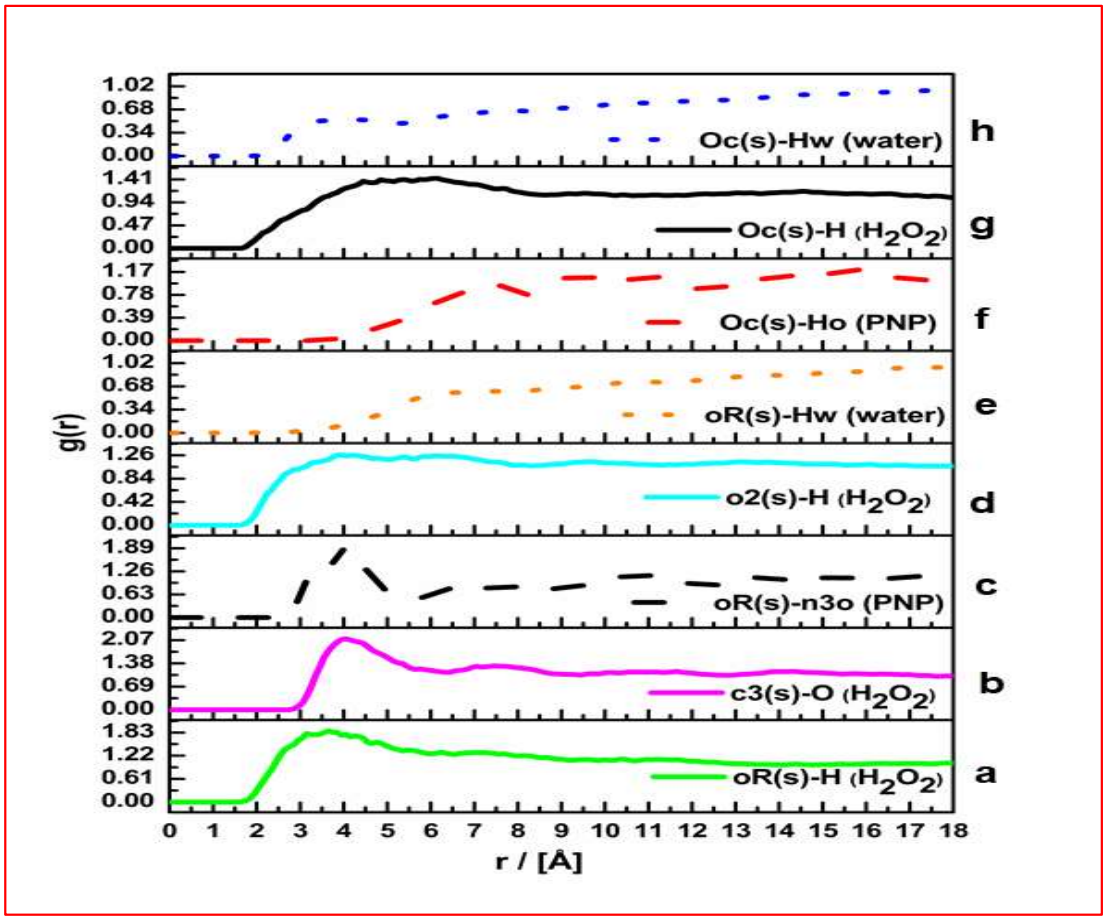

Figure 4.10 The radial distribution function of different atom types in starch with those in PNP, H_2O_2, and water in the SMC system.

The interaction energy calculated for the SMC system is -756.97 kcal, substantially larger (more negative) than for the MC system (-273.57 kcal). Therefore, SMC is more stable than the MC system. It demonstrates better interaction of H_2O_2 and PNP with the SMC than with MC.

4.3.3 The heterogeneous Fenton mechanism

This section discusses a mechanism based on experimental and MD investigation evidences. The experimental results show that the Fenton activity increases manifold on using SMNPs instead of MNPs. The other experimentally obtained aspect is that starch does not have any effect on Fenton PNP degradation. Hence, H_2O_2 cleavage happens only on the magnetite surface. The final experimental information is that Fenton PNP degradation on both MNPs and SMNPs follows first-order kinetics, indicating that possibly the mechanism is the same on both catalysts.

Since starch molecules cover SMNPs, this may prevent larger PNP molecules from getting to the magnetite surface (due to steric hindrance). The RDFs from MD simulations also indicate the same in Figure 4.10. As mentioned earlier (Figure 4.10), the H_2O_2 molecules are nearest to the starch stabilized magnetite cluster, and PNP units are about 1 Å farther away. The PNP molecules not reaching the SMNPs surface means that it and H_2O_2 molecules cannot occupy adjacent sites on the catalyst surface as required by a classical Langmuir-Hinshelwood type mechanism. Consequently, a Langmuir-Hinshelwood type mechanism is ruled out.

Classical MD investigations also reveal that PNP molecules mainly surround the magnetite cluster with only a few H_2O_2 molecules on its surface. Experimental results show that heterogeneous Fenton activity on MNPs is much lower than that observed on SMNPs. Hence, one can conclude that this spatial distribution of PNP molecules around

MNPs is not favorable to Fenton activity. In other words, the primary criterion for heterogeneous Fenton reaction to happen is the cleavage of H_2O_2 for hydroxyl radical formation, and that process is impeded when PNP molecules surround the MC unit.

The MD results of the SMC system show that the starch stabilized magnetite unit is surrounded mainly by the much smaller H_2O_2 molecules, though PNP molecules are also in the vicinity. The smaller H_2O_2 units, because of their increased interaction with the amylose units, reach the surface of the magnetite surface and undergo dissociation to hydroxyl radicals. These hydroxyl radicals then diffuse to regions near the SMC surface and oxidize the PNP molecules nearby. Thus, only the H_2O_2 molecules undergo cleavage at the catalyst surface while PNP remains in the vicinity. The overall sequence of events for efficient heterogeneous Fenton activity on SMNPs resembles the Eley-Rideal mechanism description [Liang et al. (2012), Furman et al. (2009), Sannino et al. (2013), Mukherjee & Sinha (2009)].

4.4 Conclusions

An attempt has been made to understand whether the mechanism of heterogeneously catalyzed Fenton reaction on the surface of MNPs and SMNPs is Langmuir-Hinshelwood or Eley-Rideal type. Experimental evidence tells us that starch stabilization of magnetite nanoparticles increases its Fenton catalytic activity for PNP degradation significantly in comparison to that on MNPs. The PNP degradation follows first-order kinetics over both catalysts, indicating that the Fenton mechanism remains the same. Classical MD simulations of the interaction of the reactants with a magnetite cluster in aqueous environment revealed that PNP predominantly surrounds the surface of the catalyst. On the other hand, the simulation with a starch stabilized magnetite cluster shows that H_2O_2 dominates its surroundings with PNP in its vicinity. Since kinetics of PNP degradation is much faster on SMNPs, therefore, the adsorption of H_2O_2 is the driving force for the

reaction. Once H_2O_2 is reduced to hydroxyl radicals, then it attacks the PNP molecules nearby. Thus, an ER type mechanism operates during the Fenton degradation of PNP over SMNPs.